
Article:
Dorgham, AK, Wang, C orcid.org/0000-0002-4301-3974, Morina, A orcid.org/0000-0001-8868-2664 et al. (1 more author) (2019) 3D tribo-nanoprinting using triboreactive materials. Nanotechnology, 30 (9). 095302. ISSN 0957-4484

https://doi.org/10.1088/1361-6528/aaf70c

3D tribo-nanoprinting using triboreactive materials

IOP Nanotechnology
Vol. X (2018), pp. 1–12

Dorgham et al.
ISSN XXX-XXXX-XXXX

3D tribo-nanoprinting using triboreactive materials

Abdel Dorgham*, Chun Wang, Ardian Morina and Anne Neville
Institute of Functional Surfaces, School of Mechanical Engineering, University of Leeds, Leeds LS2 9JT, United Kingdom

Tribology: the science of friction, wear and lubrication has never been associated in a positive way with the ability to manufacture at the nanoscale. Triboreactivity, when the contact between two surfaces promotes a chemical reaction, has been harnessed in this study to create highly tenacious nano-features. The reported 3D tribo-nanoprinting methodology has been demonstrated for organic and inorganic fluids on steel and silicon substrates and is adaptable through the interface tribology. The growth rate, composition and shape of the printed features were all found to be dependent on the nature of the printing liquid and shearing interfaces in addition to the applied temperature and contact force. The reported methodology in this study opens unprecedented future possibilities to utilize the nanoprinted films for the expanding fields of microelectronics, medical devices, flexible electronics and sensor technologies.

Keywords: *3D tribo-nanoprinting, ZDDP antiwear, DDP, tribopolymerization, AFM*

Introduction

Scanning probe techniques such as AFM have been used since the first invention of Scanning Tunneling Microscope (STM) in the early 1980s [1] to image and manipulate molecules on surfaces. Furthermore, using these techniques, complex structures can be built up through a series of selective nanoetching [2–4], nanoshaving [5, 6] and nanografting [7, 8]. In addition, these techniques have often been used to externally induce self-assembled monolayers in order to create patterned and selectively chemically functionalized layers on a wide range of surfaces [9]. These broad classes of technologies, which use scanning probe techniques such as AFM to create patterns on surfaces, are referred to as Scanning Probe Lithography (SPL) [10]. Several extensive reviews of nanopatterning using SPL techniques are already available [10–13].

In addition to nanopatterning, the AFM as a particular variation of scanning probe methodologies has been used in the last few years to advance the understanding of key tribological processes at the single-asperity contacts. For instance, Dorgham et al. [14, 15] used the AFM probe as a mechanical indenter to assess the rheological properties of the reaction film that forms on lubricated contacts when tribo-induced chemical reactions occur at high applied contact pressures and temperatures. In a seminal paper by Gosvami et al. [16], they quantified the formation kinetics of these triboreactive films and their ability to form under rubbing between the AFM probe and different substrates in a range of contact conditions.

A manufacturing revolution continues to take place as new 3D printing methodologies are devised to work across a range of scales and with the suitability to create high fidelity structures. 3D printing at the nanoscale is currently dominated by local oxidation [10] and dip-pen [17–19] nanolithography processes. In addition, direct writing techniques have also been developed to create unique sub-100nm 3D structures by converting surface bound molecules of various organometallic precursors into the gas phase then redepositing them by a focused electron beam [20, 21].

A different and new approach to achieve 3D tribo-nanoprinting, in the form of a scanning probe writing methodology, is also possible through combining the knowledge of tribochemistry and harnessing this as a manufacturing process. The principles of this newly proposed 3D tribo-nanoprinting are the following:

- "tribo" activation of a reaction occurs by the influence of contact and shear rate between the scanning tip, the surface and the chemical constituents of the carrier fluid.
- Reactions do not take place without the influence of contact/tribology, which enables selective tribochemical growth.
- Contacting conditions of applied load and temperature can be used to control the growth rate of the printed tracks.

In this paper, we will demonstrate the capabilities of this proposed 3D tribo-nanoprinting methodology by printing different inorganic and organic layers on steel and silicon substrates. Furthermore, we will present how the layers form as a function of applied load and temperature, and discuss how this can be harnessed as a versatile and controllable means of producing cheap 3D architectures for many expanding fields including flexible electronics and sensor technologies.

*Corresponding author:
Abdel Dorgham (a.dorgham@leeds.ac.uk)

IOP Nanotechnology
Vol. X (2018), pp. 1–12

ISSN XXX-XXXX-XXXX

Materials and methods

Tribo-nanoprinting relies on building 3D structures from the intermediate contact between an asperity scale tip (here the AFM tip), a substrate and the reactive component in the liquid medium. For the tribo-nanoprinting to be fully exploited, there is a necessity to understand the link between the tribocontact conditions and resulting growth of the layers for a range of substrates, e.g. steel and silicon, and triboreactive media, e.g. organic and inorganic, as discussed in detail below.

Organic liquid media

Three mixtures of low concentrations (3.0 wt.%) were prepared using three organic monomers of butyl acrylate, vinyl acetate and diallyl phthalate, as listed in Fig. 1a. The carrier fluid for the monomers used in this study was hexadecene ($CH_3(CH_2)_{14}CH_3$). The monomers and fluid carrier were commercially available from Sigma-Aldrich. Apart from diallyl phthalate (purity > 97%), the remaining monomers have high purity (> 99%) with a small amount, i.e. 3-60 ppm, of monomethyl ether hydroquinone as inhibitor to prevent auto-polymerization. The inhibitor can be removed by washing the monomer solution using the method described elsewhere [22]. However, this was not followed in order to investigate whether the tribopolymerization proceeds by pure tribochemical reaction between the monomer and substrate or by thermal initiation.

Inorganic liquid media

Three inorganic liquid mixtures were prepared; one contains secondary zinc dialkyldithiophosphate (ZDDP), the second contains a 50:50 wt.% binary mixture of ZDDP and molybdenum dithiocarbamate (MoDTC), and the third contains ashless dialkyldithiophosphate (DDP) additive, as listed in Fig. 1b. The amount of inorganic components were added such that the concentration of phosphorus in the carrier fluid is fixed at 0.8 wt.%. The carrier fluid used to mix the inorganic components was poly-α-olefin (PAO) synthetic oil of 4 cSt kinematic viscosity at 100 °C.

Substrates

To investigate the effect of substrate on the 3D tribo-nanoprinting capabilities, two surfaces were used. One is

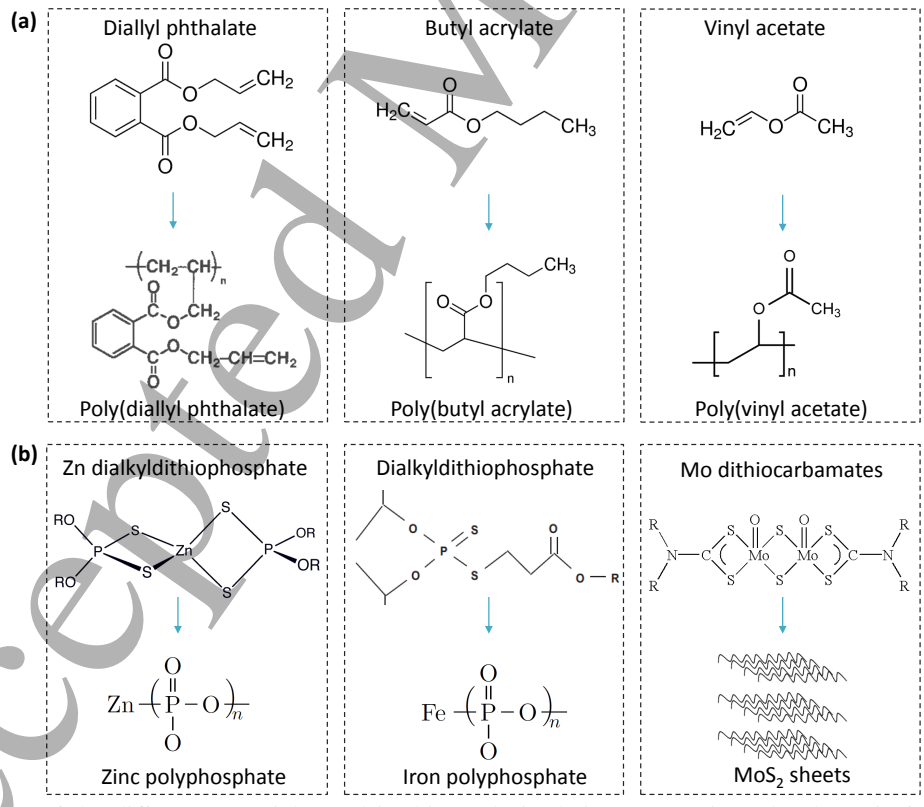

Figure 1. Structures of the different materials used in this study in their monomeric and polymeric forms. a) Monomeric and polymeric forms of butyl acrylate, vinyl acetate and diallyl phthalate mixed with hexadecene carrier fluid. b) Monomeric ZDDP, DDP and MoDTC additives mixed with PAO base oil and the composition of the formed triboreactive films of polyphosphate under rubbing.

IOP Nanotechnology
Vol. X (2018), pp. 1–12

ISSN XXX-XXXX-XXXX

a standard AISI 52100 bearing steel, which is polished to a nominal root mean square (RMS) roughness of about 10 nm and has average hardness of 64 on Rockwell scale. The second substrate is a polished crystalline silicon wafer of RMS roughness better than 0.2 nm.

AFM setup

The tribo-nanoprinting was performed in the carrier fluids using an in-house developed high temperature AFM liquid cell. The cell consists of an aluminum body where the sample under study can be glued in the center. Bolts were also used to fix the sample to avoid any drift due to the high contact pressures used during the nanoprinting. The liquid cell itself was mounted on the stage of Dimension Icon AFM (Bruker, USA) using magnets. The AFM tips used in this study were Rtespa 300 (Bruker, USA), which have a nominal radius of 8 nm and are made of antimony (n) doped Si. The AFM cantilevers were made of the same material as the tips and have a nominal spring constant of 40 N/m.

The tribo-nanoprinting was performed using AFM contact mode. Using this mode, the raster scanning was performed using different numbers of lines, i.e. from 1 to 64 lines. The scanning speed was fixed at 400 μm/s. After a certain number of scanning cycles, the nanoprinting was interrupted in order to image a bigger area using a much smaller contact force, $<$ 100 nN, capturing the rubbed and non-rubbed areas at a small scanning speed $<$ 40 μm/s.

The captured images were analyzed using Gwyddion v2.47 software. The analysis of the tribo-nanoprinting process included that quantification of the kinetics of the 3D track build-up, the shape of the track and the link between the "tribo" (contact) conditions and growth of the printed tracks.

Results

It was from the study of ZDDP and DDP as antiwear additives and the importance of tribochemistry as such that the idea of tribo-nanoprinting has emerged. Hence, we first report triboreactive printing using inorganic additives under different applied pressures and temperatures on steel and silicon substrates. These include ZDDP, DDP and a mixture of ZDDP and MoDTC. Following this, the tribopolymerization of different organic monomers will be discussed.

ZDDP triboreactive films

To demonstrate the 3D tribo-nanoprinting capabilities, Fig. 2 shows different features printed using the ZDDP additive in PAO base oil. For instance, in Fig. 2a, three letters (I, F and S), which are the initial letters of Institute of Functional Surfaces, in addition to letter E were printed at different scales. The build-up of the printed track on a single line formed by a repetitive action is shown in Fig. 2b for up to 19000 cycles of rubbing. Furthermore, the changes in topography over sliding cycles across and along a single printed line are shown in Fig. 2b. It is evident that the line thickness and area increase rapidly as rubbing cycles increase. The rates of formation of the tracks are discussed later. The increase in area suggests that the tribofilm does not only form under the AFM tip but can also flow to the sides. Another observation is related to the uniformity of the formed line. Over the sliding cycles, the formed triboreactive film appears uneven and patchy along its length. One explanation for this behavior can be related to the disruption caused by the reciprocating motion of the AFM tip over a very short period of time while the film is susceptible to deformation. In addition, this can be related to load instability [23] as the AFM tip changes direction as well as to any surface heterogeneity [16]. It should be noted that the build-up of these printed tracks is being achieved by a tribochemical reaction. The controlling factors are the contact forces, rubbing mechanism (smooth sliding or stick/slip) and the resulting triboactivation of reactions that occur between the tip and surface. Furthermore, the physical and chemical nature of the surface, i.e. mechanochemical properties, has already been shown, in several tribology-related publications, to affect the nature and kinetics of the tribofilm build-up [24, 25].

To test the effect of substrate, Fig. 2c and d show the evolution of the structure of different printed ZDDP triboreactive films on steel and silicon substrates, respectively, using 2, 4 and 8 lines raster scanning an area of $5 \times 5\,\mu m^2$. The formed films whether on steel or silicon substrate showed several distinctive features. Initially, the edges of the formed films appear to be thicker than the areas in the middle. This continues to be the case until the end of the printing process. The reason for this enlarged thickness can be related to the larger number of sliding cycles experienced near the edges due to the narrower gap between the adjacent scanning lines, which causes double rubbing action at these regions as the scanning lines get closer to each other and finally overlap when moving towards the edges. Another possibility can be related to the change in the direction of scanning near the edges, which can change the speed profile such that the lubrication regime near the edges becomes more severe, i.e. boundary lubrication. Harsher conditions are known to cause a higher formation rate [26].

One of the main differences between the films formed on steel and silicon substrates is the smaller formation rate in the case of silicon compared to steel. For instance, after 6000 cycles, the thickness of the formed tracks on steel was about 30 nm (Fig. 2c) compared to only about 5 nm in the case of silicon substrate (Fig. 2d). Same observation can be found by comparing the thickness of the formed tracks after 18000 cycles, which was about 120 nm in the case of steel (Fig. 2b) whereas only 10 nm in the case of silicon (Fig. 2d). The low reactivity and formation rate on the silicon substrate can

IOP Nanotechnology
Vol. X (2018), pp. 1–12

ISSN XXX-XXXX-XXXX

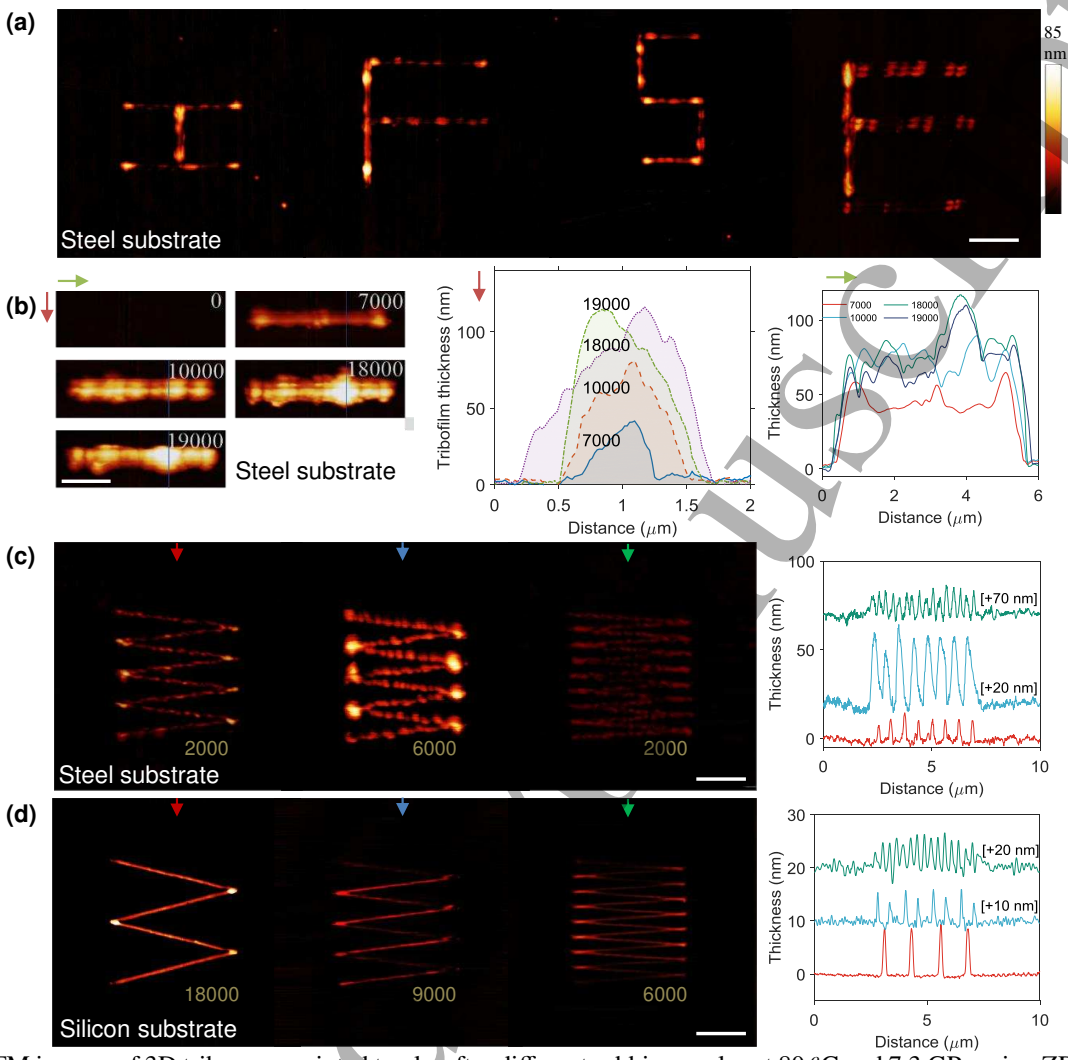

Figure 2. AFM images of 3D tribo-nanoprinted tracks after different rubbing cycles at 80 ^{o}C and 7.3 GPa using ZDDP additive in PAO base oil. a) Different printed letters on steel substrate at various scales, b) Single printed track on steel substrate and its profile evolution across and along the printed line over rubbing cycles. c) and d) Different printed features on steel and silicon substrates, respectively, and their profile evolutions across the printed tracks over rubbing cycles. The shown scale bar on all the AFM images represents 2 μm.

explain the reason behind the maintained good quality of the AFM images without much effect of any films formed on the AFM tip, as it is made of silicon and thus small films can be formed on it. The good quality of the AFM images can also be related to the low tenacity of the films formed on silicon, as shown Fig. 2d, that can be easily removed.

Another feature appears specifically in the films formed on the steel substrate, which is related to the high roughness of these films compared to the one of the films formed on silicon. It seems that this behavior is causes by the higher roughness of the steel substrate, i.e. about 10 nm, than the Si substrate, i.e. better than 0.2 nm. The enhanced roughness of the printed triboreactive films indicates that they are formed initially on the contacting asperities at which higher local loads and temperatures are encountered. Load and temperature are known to cause drastic increase in the growth rate of the triboreactive films [15, 16, 27]. It follows that thicker localized areas of the film will grow before others on the rough steel surface, which eventually results in the formation of films with high surface roughness.

ZDDP and MoDTC triboreactive films

One of the measures to reduce friction in engineering components, e.g. engines for automobile, is the use of oil additives such as MoDTC. The MoDTC molecules decompose at high temperature and under shear to form MoS_2 sheets on the contacting surfaces, which reduce friction due to their

IOP Nanotechnology
Vol. X (2018), pp. 1–12

ISSN XXX-XXXX-XXXX

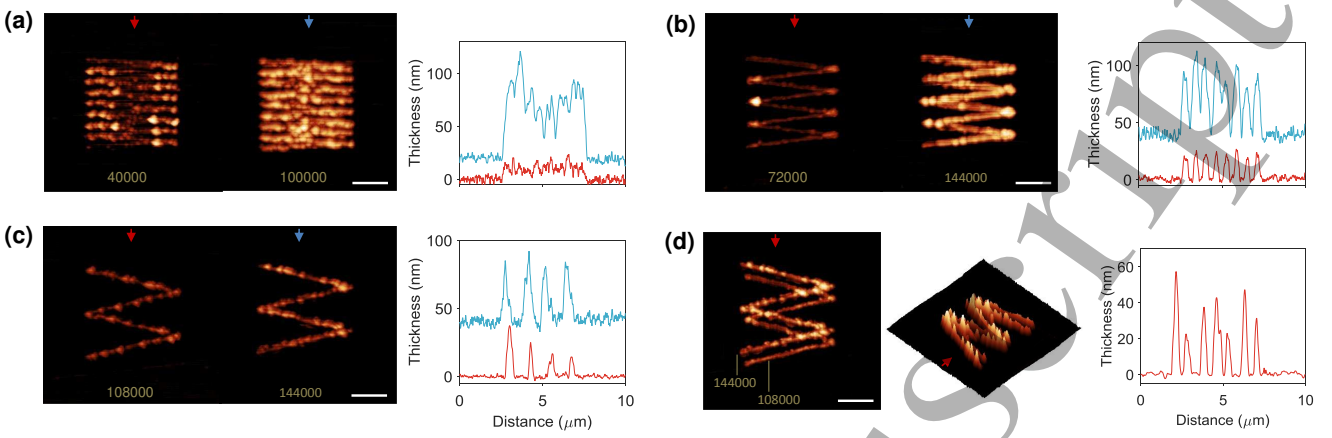

Figure 3. AFM images of 3D tribo-nanoprinted tracks formed on silicon substrate after different rubbing cycles at 80 ^{o}C and 4.6 GPa using a 50:50 wt.% mixture of ZDDP and MoDTC additives in PAO base oil. a-d) Printed films using 8, 4, 2 and double 2 scanning lines, respectively, and their profile evolutions across the printed tracks over rubbing cycles. The shown scale bar on all the AFM images represents 2 μm.

low shear strength [28] originated from the facilitated interlayer sliding by the large interlayer Coulombic repulsive interactions [29]. The formed sheets are typically few molecular layers thick [30]. Apart from the antiwear ZDDP additive, adding MoDTC as a friction modifier can help protect the probe and facilitate printing for elongated periods. In order to examine the effects of these sheets on the tribo-nanoprinting capabilities, Fig. 3 presents the evolution of different printed features on silicon substrate using a binary 50:50 wt.% mixture of ZDDP and MoDTC. The formed films showed several distinctive features. First, similar to the ZDDP films, the edges of the formed films appear to be thicker than the areas in the middle, which can be related to the larger number of sliding cycles experienced near the edges as the scanning lines overlap when the AFM tip moves towards the edges. Second, the large edges can be easily removed over sliding cycles, which indicates that the films are soft. Third, the formed films appear discontinuous and have high surface roughness compared to the smooth ZDDP films formed on silicon substrate (Fig. 2d). As this behavior is typically observed in the case of formed films on rough surfaces (e.g. ZDDP on steel in Fig. 2c), this may suggest that the MoDTC adsorbs initially to the silicon substrate, decomposes to form MoS_2 discontinuous sheets on the contacting surfaces [30] and subsequently forms interlocked layers of MoS_2 and zinc phosphate of large effective roughness. The MoS_2 impregnated in the phosphate containing tracks has important properties such as low shear strength [28] as discussed earlier and diamagnetic characteristics [31]. This brings the potential for the printed tracks to have different functional behavior.

DDP triboreactive films

In order to investigate the effect of Zn and Fe cations on the printing capabilities, different features were printed using ashless DDP additive in PAO base oil rubbed on steel and silicon substrates, as shown in Fig. 4. In the case of large number of lines, i.e. 8, are printed on the steel substrate (Fig. 4a), the DDP films formed during the early stage of printing appear to have larger thickness near the edges compared to the central region, which is similar to the case of the ZDDP films formed on steel substrates. The non-uniform thickness seems to depend mainly on the initially formed regions, which keep growing more than the rest of the triboreactive film. The double rubbing action at these regions due to the overlapping scanning lines as they get closer to the edges appears to be the main reason behind this phenomenon, as discussed earlier. As rubbing cycles progressed, further shearing seems to induce more formation in the central regions until matching the ones on the sides.

When a fewer number of lines, i.e. 4, were printed on the steel substrate (Fig. 4b), the film did not appear to have larger thickness near the edges compared to the central region. Instead, a uniform and continuous film structure was formed throughout the tribo-nanoprinting. Using 4 instead of 8 scanning lines raster scanning an area of $5 \times 5\,\mu m^2$ results in a maximum separation distance between the adjacent lines of about 1.25 μm instead of 625 nm. The doubled distance ensured that less overlapping between the adjacent lines occurs near the edges, which in turn results in a more uniform tribofilm.

Rubbing seems to increase not only the thickness but also the width of every printed line as suggested by the profile evolution across a single line as shown in Fig. 4c. Wear and smearing of the printed DDP lines under high contact pres-

IOP Nanotechnology
Vol. X (2018), pp. 1–12

ISSN XXX-XXXX-XXXX

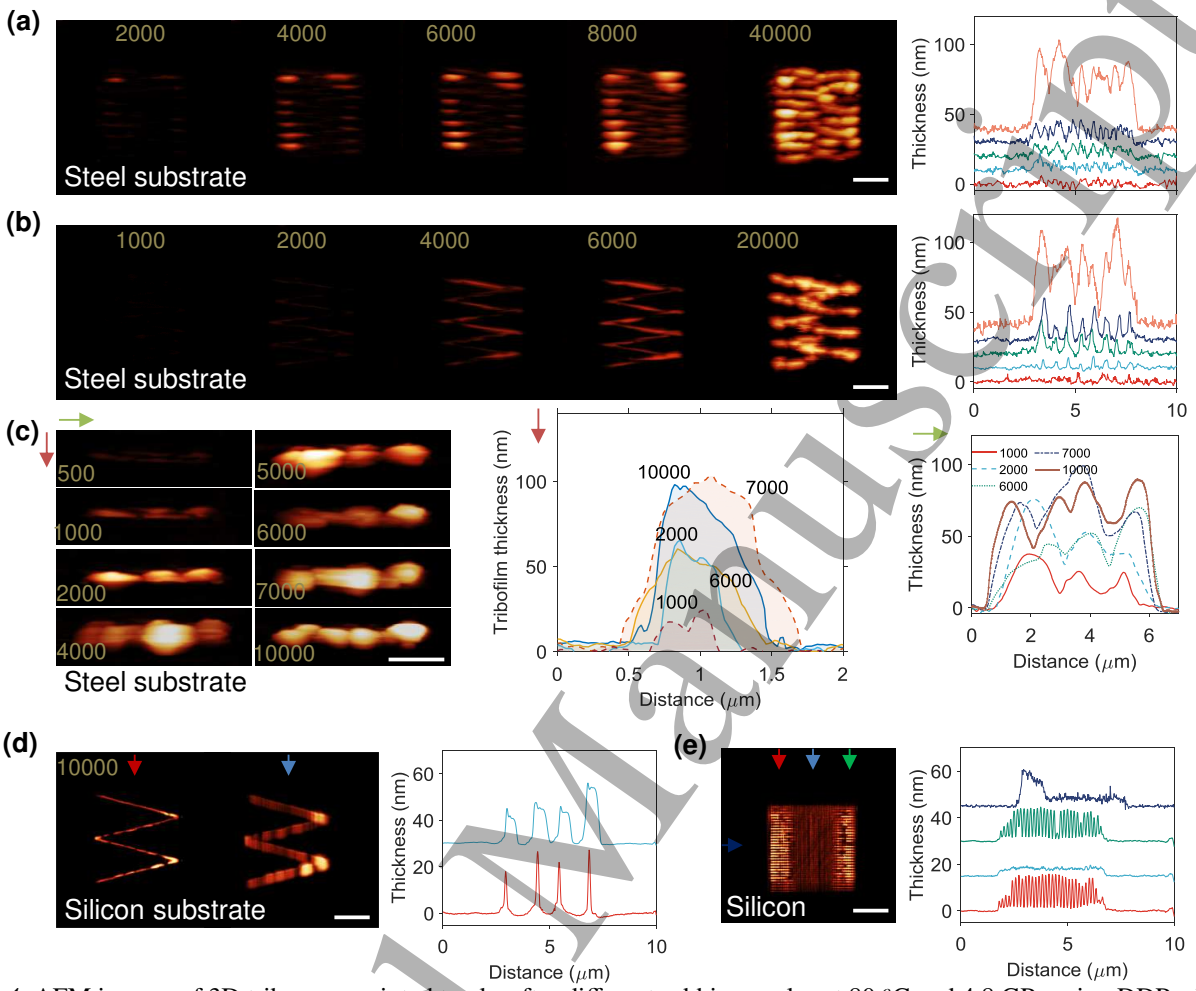

Figure 4. AFM images of 3D tribo-nanoprinted tracks after different rubbing cycles at 80 ^{o}C and 4.8 GPa using DDP additive in PAO base oil. a,b) Different printed features on steel substrate using 8 and 4 scanning lines, respectively, and their profile evolutions across the printed track over rubbing cycles. c) Single printed track on steel substrate and its profile evolution across and along the printed line over rubbing cycles. d) and e) Different printed features on silicon substrate using 2 and 32 scanning lines, respectively, and their profile evolutions across the printed tracks. The shown scale bar on all the AFM images represents 2 μm.

sure might be responsible for enlarged width although there is a lack of evidence to support it. Another possible cause can be related to the flowability of the formed lines, which is supported by the continuous spread of the formed films until they fill the whole region even between adjacent lines where no rubbing occurs. Finally, as rubbing progressed, the thick areas along the lines can disintegrate into smaller ones. This becomes evident by noticing the change in the profile between 7000 and 10000 cycles.

To test the effect of substrate, Fig. 4d shows the evolution of the structure of the printed DDP triboreactive film on a silicon substrate using 2 and 4 lines raster scanning an area of $5 \times 5\,\mu m^2$. The formed films appear to be of low roughness compared to the ones formed on steel. As discussed in the case of ZDDP, this behavior seems to originate from the higher roughness of the steel than silicon substrate.

It is interesting to observe that when the printed DDP lines were scanned under large contact pressure of about 4.8 GPa, the ultrathin lines in the lateral direction become wider (Fig. 4d). This was not observed in the case of the ZDDP films. This behavior can be related to the phosphate type forming the main bulk of the printed film. The formed triboreactive films in the case of ZDDP on silicon substrates consist mainly of long chains of zinc phosphate whereas in the case of DDP on silicon a phosphate matrix of mainly short chains, which possibly contains Si as modifier cation, is formed instead. Thus, the type of available cations during the decomposition of the additive seems to affect not only the composition but also the structure and tenacity of the printed tracks.

IOP Nanotechnology
Vol. X (2018), pp. 1–12

ISSN XXX-XXXX-XXXX

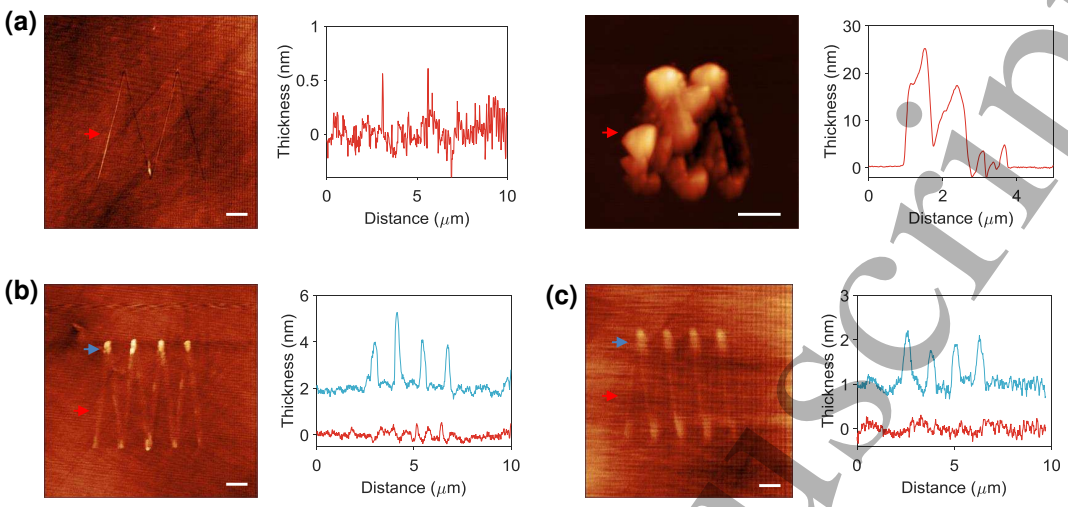

Figure 5. AFM images of 3D tribo-nanoprinted tracks after different rubbing cycles at 25 ^{o}C and 4.6 GPa on silicon substrate using different monomers in hexadecene carrier fluid. a-c) Different features printed using diallyl phthalate, vinyl acetate and butyl acrylate, respectively, and their profile evolutions across the printed tracks. The shown scale bar on all the AFM images represents 1 μm.

Monomer tribopolymerization

As demonstrated in the previous sections, printing inorganic layers from the ZDDP and DDP molecules is possible and relies on an inorganic polymerization to form phosphate glass. In this section, we exploit the idea of tribo-nanoprinting by tribopolymerization of organic polymers, which to our best knowledge has never been implemented before. The tribo-nanoprinting of different features using several monomers is shown in Fig. 5 for the case of diallyl phthalate (Fig. 5a), vinyl acetate (Fig. 5b) and butyl acrylate (Fig. 5c). The tracks are formed through the tribopolymerization of the monomers by the action of rubbing [32–35]. The biggest growth was observed in the case of diallyl phthalate (Fig. 5a) as sliding seems to enhance the polymerization of the monomers to the extent that it appeared as if covering the entire scanned area including the areas between the scanning lines where no rubbing took place. This behavior can be related to the flowability and solidification of the printed polymer as it is formed.

The limited growth of the polymers in the cases other than diallyl phthalate can be mainly related to the small amount, i.e. 3-60 ppm, of monomethyl ether hydroquinone inhibitor in the monomer.

Discussion

Nanoprinting mechanism using inorganic P-based additives

The 3D tribo-nanoprinting discussed in this study relies on utilizing the tribological rubbing to induce chemical reactions between reactive additives in a fluid carrier and rubbing surfaces. The schematic diagrams shown in Fig. 6 helps explain the evolution of the 3D nanoprinting mechanisms over rubbing cycles. In the case of printed triboreactive films using inorganic P-based oil additives such as ZDDP and DDP, the formation of the films seems to undergo three main stages as shown in Fig. 6b. The proposed mechanism suggests that the first step before forming the printed films is the adsorption of the additive molecules to the substrate, whether a steel [15, 16, 36] or silicon [16] surface. Rubbing under high contact pressure and temperature can then cause the adsorbed molecules to decompose partially on the contacting asperities by losing sulfur to form a discontinuous sulfur-rich layer, which can be considered as active sites on the surface that help promote the subsequent growth steps [15, 37–46]. Further rubbing causes the adsorbed molecules on the active sites to decompose completely to form phosphate species in the form of a two-dimensional network of chains progressively increasing in length [37, 38, 47]. The formed phosphate films in the case of ZDDP rubbed on Fe or Si substrate consist mainly of zinc phosphate of relatively long chains, i.e. $n = 2 - 5$ [48]. On the other hand, in the case of DDP on Si or Fe, a phosphate matrix of short chains, which might contain Si or Fe modifier cations, is formed [49–53]. Any harsh conditions of high temperature and large contact pressure or even just long rubbing or heating time can cleave any formed long phosphate chains into shorter ones [54].

During the tribo-nanoprinting process, the decomposition reaction of P-based additives to form triboreactive films was found to be activated using heat and/or shear at high contact pressure, as shown in Fig. 7 for the case of ZDDP and DDP. Thus, the full control of the formation kinetics and di-

IOP Nanotechnology
Vol. X (2018), pp. 1–12

ISSN XXX-XXXX-XXXX

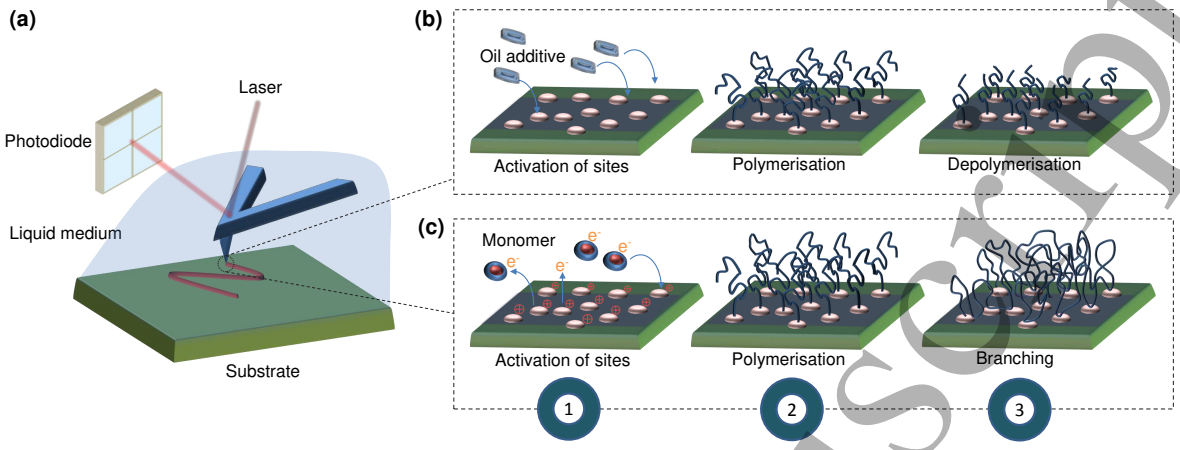

Figure 6. Schematics of the 3D tribo-nanoprinting mechanism. a) AFM liquid cell used during the nanoprinting. b) and c) Evolution of the printed triboreactive films using P-based inorganic oil additives and tribopolymerized organic monomers, respectively, over rubbing cycles.

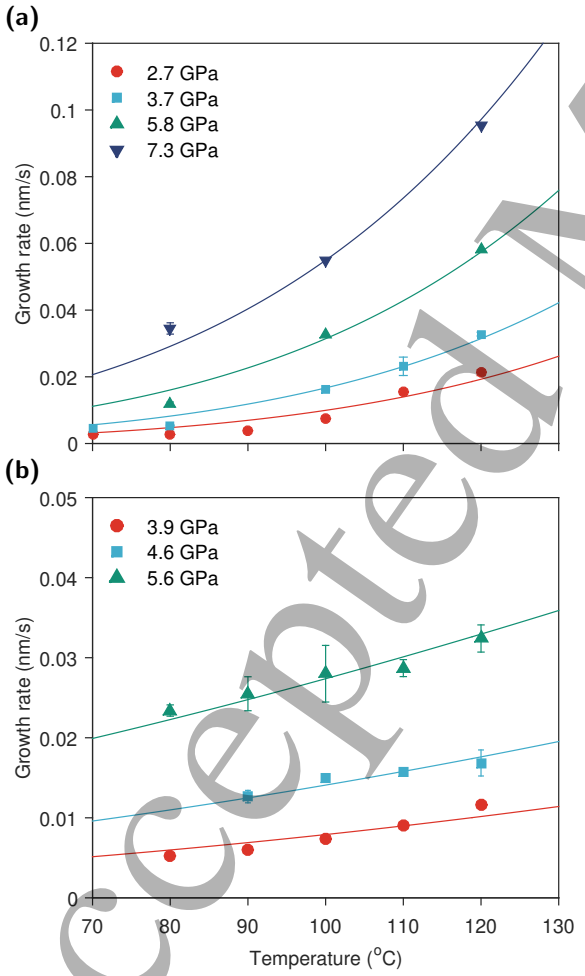

Figure 7. Evolution of the growth rate of a) ZDDP and b) DDP triboreactive films over different levels of contact pressure and temperature. Solid lines are exponential fits.

mensions of the printed features is possible by utilizing the synergy between these two factors.

Nanoprinting mechanism using organic monomers

The results of this study show that the different tested monomers can be polymerized under rubbing to form thin films of polymeric nature at the contacting surfaces, which is in line with the findings of several previous studies [32–35, 55–58]. The rubbing-induced polymerization process is called tribopolymerization [33]. The tribopolymerization of monomers and how it is initiated and propagated under rubbing conditions to form polymeric films on the contacting surfaces can be explained according to the negative ion-radical action mechanism (NIRAM) [56], as demonstrated in the schematic diagram in Fig. 6c. The NIRAM model suggests that initially rubbing causes electrons to be generated from the contacting surfaces. The exoelectron emission was verified for different surfaces [59]. The emitted electrons appear to have low energy, i.e. < 5 eV. These electrons, which may fall under different categories depending on their origin and energy [60], can contribute significantly to the tribochemical reactions [55, 56, 59, 61–64]. First, as they leave the metal surface, they create positively charged activation sites. Second, they can react with the monomer molecules, which results in the formation of anions and radicals. Third, the formed anions can react with the positively charged activation sites to form a polymeric film. Thus, tribopolymerization appears to be initiated under rubbing by the low-energy exoelectrons and propagated by the radicals' formation kinetics. This process explains the polymerization of the different monomers used in this study. For instance, the butyl acrylate monomer is highly reactive and can polymerize easily especially under heat and rubbing [57]. This was suggested to follow a free-radical addition polymeriza-

IOP Nanotechnology
Vol. X (2018), pp. 1–12

ISSN XXX-XXXX-XXXX

tion leading to the formation of poly(n-butyl acrylate) (PBA) with very high molecular weight (HMW) [22, 57]. Other monomers like vinyl acetate [34, 62] and diallyl phthalate [62] were also reported to be able to tribopolymerize under rubbing to form poly(vinyl acetate) and poly(diallyl phthalate), respectively, on the contacting surfaces.

The limited growth of the polymers in the cases other than diallyl phthalate can be related to the small amount of hydroquinone inhibitor, i.e. 3-60 ppm, added by the manufacturer to the monomers in order to prevent auto-polymerization. Nonetheless, the ability of the monomers to polymerize under rubbing despite the inhibitor's presence indicates, as discussed earlier, that the tribopolymerization process initiates by pure tribochemical reactions between the monomer and substrate rather than due to mere thermal activation.

Conclusion

A novel methodology was reported in this study that can be utilized to print small features at the nanoscale. Using this methodology, it was possible to print organic and inorganic features on different substrates including steel and silicon. Furthermore, it was possible to study the formation kinetics of some of the formed films under different operating conditions of temperature and contact pressure. Although the printed films were non-conductive, they can be easily made electrically conductive by dispersing amounts of, for instance, multilayer graphene [65] within the printing bath. In order to achieve electrical conductivity, the added volume fraction must be chosen such that it is above the percolation threshold.

The findings of this study broaden the horizon to utilize the presented tribo-nanoprinting methodology in, amongst other things, printing cheap nano-electronics on different hard and flexible substrates.

Acknowledgements

This work is supported by EPSRC (grant number EP/R001766/1) and Marie Curie Initial Training Networks (grant number 317334).

Author contributions statement

A.D. performed the experiments, analysed the results and prepared the manuscript. All authors reviewed the manuscript.

Additional information

Competing financial interests (The authors declare no competing interests).

References

(1) Binnig, G.; Rohrer, H. Scanning tunneling microscopy. *Surface science* **1983**, *126*, 236–244.

(2) Xia, Y.; Zhao, X.-M.; Kim, E.; Whitesides, G. M. A selective etching solution for use with patterned self-assembled monolayers of alkanethiolates on gold. *Chemistry of materials* **1995**, *7*, 2332–2337.

(3) Schmidt, O. G.; Eberl, K. Nanotechnology: Thin solid films roll up into nanotubes. *Nature* **2001**, *410*, 168.

(4) Zhuang, D; Edgar, J. Wet etching of GaN, AlN, and SiC: a review. *Materials Science and Engineering: R: Reports* **2005**, *48*, 1–46.

(5) Garno, J. C.; Yang, Y.; Amro, N. A.; Cruchon-Dupeyrat, S.; Chen, S.; Liu, G.-Y. Precise positioning of nanoparticles on surfaces using scanning probe lithography. *Nano Letters* **2003**, *3*, 389–395.

(6) Xu, S.; Liu, G.-y. Nanometer-scale fabrication by simultaneous nanoshaving and molecular self-assembly. *Langmuir* **1997**, *13*, 127–129.

(7) Liu, M.; Amro, N. A.; Liu, G.-y. Nanografting for surface physical chemistry. *Annu. Rev. Phys. Chem.* **2008**, *59*, 367–386.

(8) Liu, J.-F.; Cruchon-Dupeyrat, S.; Garno, J. C.; Frommer, J.; Liu, G.-Y. Three-dimensional nanostructure construction via nanografting: positive and negative pattern transfer. *Nano Letters* **2002**, *2*, 937–940.

(9) Chou, S. Y.; Zhuang, L. Lithographically induced self-assembly of periodic polymer micropillar arrays. *Journal of Vacuum Science & Technology B: Microelectronics and Nanometer Structures Processing, Measurement, and Phenomena* **1999**, *17*, 3197–3202.

(10) Garcia, R.; Martinez, R. V.; Martinez, J. Nanochemistry and scanning probe nanolithographies. *Chemical Society Reviews* **2006**, *35*, 29–38.

(11) Vigneswaran, N; Samsuri, F.; Ranganathan, B., et al. Recent Advances in Nano Patterning and Nano Imprint Lithography for Biological Applications. *Procedia Engineering* **2014**, *97*, 1387–1398.

(12) Braunschweig, A. B.; Huo, F.; Mirkin, C. A. Molecular printing. *Nature chemistry* **2009**, *1*, 353.

(13) Mendes, P. M.; Yeung, C. L.; Preece, J. A. Bionanopatterning of surfaces. *Nanoscale research letters* **2007**, *2*, 373.

(14) Dorgham, A. Reaction kinetics and rheological characteristics of ultra-thin P-based triboreactive films., Ph.D. Thesis, University of Leeds, 2018.

(15) Dorgham, A.; Parsaeian, P.; Azam, A.; Wang, C.; Morina, A.; Neville, A. Single-asperity study of the reaction kinetics of P-based triboreactive films. *Tribology International* **0000**, *0*, Just Accepted.

(16) Gosvami, N.; Bares, J.; Mangolini, F; Konicek, A.; Yablon, D.; Carpick, R. Mechanisms of antiwear tribofilm growth revealed in situ by single-asperity sliding contacts. *Science* **2015**, *348*, 102–106.

(17) Piner, R. D.; Zhu, J.; Xu, F.; Hong, S.; Mirkin, C. A. " Dip-pen" nanolithography. *science* **1999**, *283*, 661–663.

(18) Salaita, K.; Wang, Y.; Mirkin, C. A. Applications of dip-pen nanolithography. *Nature nanotechnology* **2007**, *2*, 145.

(19) Ginger, D. S.; Zhang, H.; Mirkin, C. A. The Evolution of dip-Pen nanolithography. *Angewandte Chemie International Edition* **2004**, *43*, 30–45.

(20) Höflich, K.; Yang, R. B.; Berger, A.; Leuchs, G.; Christiansen, S. The Direct Writing of Plasmonic Gold Nanostructures by Electron-Beam-Induced Deposition. *Advanced Materials* **2011**, *23*, 2657–2661.

(21) Shawrav, M. M.; Taus, P.; Wanzenboeck, H. D.; Schinnerl, M; Stöger-Pollach, M; Schwarz, S; Steiger-Thirsfeld, A; Bertagnolli, E. Highly conductive and pure gold nanostructures grown by electron beam induced deposition. *Scientific reports* **2016**, *6*, 34003.

(22) Ahmad, N. M.; Heatley, F.; Lovell, P. A. Chain transfer to polymer in free-radical solution polymerization of n-butyl acrylate studied by NMR spectroscopy. *Macromolecules* **1998**, *31*, 2822–2827.

(23) Aktary, M.; McDermott, M.; McAlpine, G. Morphology and nanomechanical properties of ZDDP antiwear films as a function of tribological contact time. *Tribology letters* **2002**, *12*, 155–162.

(24) Neville, A; Morina, A; Haque, T; Voong, M Compatibility between tribological surfaces and lubricant additives–how friction and wear reduction can be controlled by surface/lube synergies. *Tribology International* **2007**, *40*, 1680–1695.

(25) Vengudusamy, B.; Green, J. H.; Lamb, G. D.; Spikes, H. A. Tribological properties of tribofilms formed from ZDDP in DLC/DLC and DLC/steel contacts. *Tribology International* **2011**, *44*, 165–174.

(26) Shimizu, Y.; Spikes, H. A. The tribofilm formation of ZDDP under reciprocating pure sliding conditions. *Tribology Letters* **2016**, *64*, 46.

(27) Yin, Z.; Kasrai, M.; Fuller, M.; Bancroft, G. M.; Fyfe, K.; Tan, K. H. Application of soft X-ray absorption spectroscopy in chemical characterization of antiwear films generated by ZDDP Part I: the effects of physical parameters. *Wear* **1997**, *202*, 172–191.

(28) Graham, J.; Spikes, H.; Korcek, S. The friction reducing properties of molybdenum dialkyldithiocarbamate additives: part I—factors influencing friction reduction. *Tribology Transactions* **2001**, *44*, 626–636.

(29) Onodera, T.; Morita, Y.; Suzuki, A.; Koyama, M.; Tsuboi, H.; Hatakeyama, N.; Endou, A.; Takaba, H.; Kubo, M.; Dassenoy, F., et al. A computational chemistry study on friction of h-MoS_2. Part I. Mechanism of single sheet lubrication. *The Journal of Physical Chemistry B* **2009**, *113*, 16526–16536.

(30) De Barros' Bouchet, M.; Martin, J.; Le-Mogne, T; Vacher, B Boundary lubrication mechanisms of carbon coatings by MoDTC and ZDDP additives. *Tribology International* **2005**, *38*, 257–264.

(31) Tongay, S.; Varnoosfaderani, S. S.; Appleton, B. R.; Wu, J.; Hebard, A. F. Magnetic properties of MoS 2: existence of ferromagnetism. *Applied Physics Letters* **2012**, *101*, 123105.

(32) Furey, M. The formation of polymeric films directly on rubbing surfaces to reduce wear. *Wear* **1973**, *26*, 369–392.

(33) Kajdas, C.; Lafleche, P.; Furey, M.; Hellgeth, J.; Ward, T. A study of tribopolymerisation under fretting contact conditions. *Lubrication Science* **1993**, *6*, 51–89.

(34) Tripathy, B.; Furey, M.; Kajdas, C Mechanism of wear reduction of alumina by tribopolymerization. *Wear* **1995**, *181*, 138–147.

(35) Furey, M.; Tritt, B.; Kajdas, C; Kempinski, R Lubrication of ceramics by tribopolymerization: a designed experiment to determine effects of monomer structure, load, and speed on wear. *Tribology transactions* **1999**, *42*, 833–841.

(36) Fuller, M. L. S.; Kasrai, M.; Bancroft, G. M.; Fyfe, K.; Tan, K. H. Solution decomposition of zinc dialkyl dithiophosphate and its effect on antiwear and thermal film formation studied by X-ray absorption spectroscopy. *Tribology international* **1998**, *31*, 627–644.

(37) Dorgham, A.; Parsaeian, P.; Neville, A.; Ignatyev, K.; Mosselmans, F.; Masuko, M.; Morina, A. In situ synchrotron XAS study of the decomposition kinetics of ZDDP triboreactive interfaces. *RSC Advances* **2018**, *8*, 34168–34181.

(38) Dorgham, A; Neville, A; Ignatyev, K; Mosselmans, F; Morina, A An in situ synchrotron XAS methodology for surface analysis under high temperature, pressure, and shear. *Review of Scientific Instruments* **2017**, *88*, 015101.

(39) Dorgham, A.; Azam, A.; Morina, A.; Neville, A. On the Transient Decomposition and Reaction Kinetics of Zinc Dialkyldithiophosphate. *ACS Applied Materials & Interfaces* **0000**, *0*, Just Accepted.

(40) Dorgham, A; Neville, A; Morina, A In *Advanced Analytical Methods in Tribology*; Springer: 2018, pp 159–214.

(41) Martin, J. M. Antiwear mechanisms of zinc dithiophosphate: a chemical hardness approach. *Tribology letters* **1999**, *6*, 1–8.

(42) Jahanmir, S. Wear reduction and surface layer formation by a ZDDP additive. *Journal of tribology* **1987**, *109*, 577–586.

(43) Baldwin, B. A. Relationship between surface composition and wear: an X-ray photoelectron spectroscopic study of surfaces tested with organosulfur compounds. *ASLE transactions* **1976**, *19*, 335–344.

(44) Baldwin, B. Wear mitigation by antiwear additives in simulated valve train wear. *Asle Transactions* **1983**, *26*, 37–47.

(45) Sakurai, T.; Sato, K. Study of corrosivity and correlation between chemical reactivity and load-carrying capacity of oils containing extreme pressure agents. *ASLE TRANSACTIONS* **1966**, *9*, 77–87.

(46) Batchelor, A.; Cameron, A; Okabe, H An apparatus to investigate sulfur reactions on nascent steel surfaces. *ASLE transactions* **1985**, *28*, 467–474.

(47) Spikes, H. The History and Mechanisms of ZDDP. *Tribology Letters* **2004**, *17*, 469–489.

(48) Crobu, M.; Rossi, A.; Mangolini, F.; Spencer, N. D. Chain-length-identification strategy in zinc polyphosphate glasses by means of XPS and ToF-SIMS. *Analytical and bioanalytical chemistry* **2012**, *403*, 1415–1432.

(49) Zhang, Z; Yamaguchi, E.; Kasrai, M; Bancroft, G.; Liu, X; Fleet, M. Tribofilms generated from ZDDP and DDP on steel surfaces: Part 2, chemistry. *Tribology Letters* **2005**, *19*, 221–229.

(50) Kim, B.; Sharma, V.; Aswath, P. B. Chemical and mechanistic interpretation of thermal films formed by dithiophosphates using XANES. *Tribology International* **2017**, *114*, 15–26.

(51) Najman, M.; Kasrai, M; Bancroft, G.; Miller, A Study of the chemistry of films generated from phosphate ester additives on 52100 steel using X-ray absorption spectroscopy. *Tribology Letters* **2002**, *13*, 209–218.

(52) Najman, M.; Kasrai, M; Bancroft, G. Chemistry of antiwear films from ashless thiophosphate oil additives. *Tribology Letters* **2004**, *17*, 217–229.

(53) Najman, M.; Kasrai, M; Bancroft, G.; Frazer, B.; De Stasio, G The correlation of microchemical properties to antiwear (AW) performance in ashless thiophosphate oil additives. *Tribology Letters* **2004**, *17*, 811–822.

(54) Heuberger, R.; Rossi, A.; Spencer, N. D. Pressure dependence of ZnDTP tribochemical film formation: a combinatorial approach. *Tribology Letters* **2007**, *28*, 209–222.

(55) Kajdas, C. K. Importance of the triboemission process for tribochemical reaction. *Tribology International* **2005**, *38*, 337–353.

(56) Kajdas, C; Hiratsuka, K Tribochemistry, tribocatalysis, and the negative-ion-radical action mechanism. *Proceedings of the Institution of Mechanical Engineers, Part J: Journal of Engineering Tribology* **2009**, *223*, 827–848.

(57) Zheng, J.; Zhang, L.; Du, Z.; Zhang, C.; Li, H. Tribopolymerization of n-butyl acrylate on the steel–steel rubbing surface. *Tribology International* **2008**, *41*, 769–777.

(58) Svahn, F.; Csillag, S. Formation of low-friction particle/polymer composite tribofilms by tribopolymerization. *Tribology letters* **2011**, *41*, 387–393.

(59) Molina, G. J.; Furey, M. J.; Ritter, A.; Kajdas, C. Triboemission from alumina, single crystal sapphire, and aluminum. *Wear* **2001**, *249*, 214–219.

(60) Oster, L; Yaskolko, V; Haddad, J Classification of exoelectron emission mechanisms. *physica status solidi (a)* **1999**, *174*, 431–439.

(61) Kajdas, C. On a negative-ion concept of EP action of organo-sulfur compounds. *ASLE transactions* **1985**, *28*, 21–30.

(62) Kajdas, C. Importance of anionic reactive intermediates for lubricant component reactions with friction surfaces. *Lubrication Science* **1994**, *6*, 203–228.

(63) Furey, M.; Ritter, A.; Molina, G. Triboemission as a basic part of the boundary friction regime: a review. *Lubrication Science* **2002**, *14*, 223–254.

(64) Dante, R. C.; Kajdas, C. A review and a fundamental theory of silicon nitride tribochemistry. *Wear* **2012**, *288*, 27–38.

(65) Chakraborty, I.; Bodurtha, K. J.; Heeder, N. J.; Godfrin, M. P.; Tripathi, A.; Hurt, R. H.; Shukla, A.; Bose, A. Massive electrical conductivity enhancement of multilayer graphene/polystyrene composites using a nonconductive filler. *ACS applied materials & interfaces* **2014**, *6*, 16472–16475.